30th AIAA Applied Aerodynamics Conference
25-28 June 2012, New Orleans, Louisiana
2012-2892

# Experimental Study of a Multielement Airfoil for Large Wind Turbines

Brent W. Pomeroy*, Gregory A. Williamson†, and Michael S. Selig‡
*University of Illinois at Urbana-Champaign, Department of Aerospace Engineering, Urbana, IL 61801*

**Large wind turbines have thick airfoils at the root section of the wind turbine to support the weight of the blade and structural requirements, and aerodynamic efficiencies are in conflict near the root section of the blades. A four-element multielement airfoil system was tested as a replacement airfoil system for a thick single element airfoil near the root of a 10-MW scale conceptual wind turbine. The system consisted of a main element, two flaps, and a lower strut airfoil element for added structural support, and experiments were performed with the ability to move two flaps to any location relative to a main element. Tests were performed in the University of Illinois low turbulence subsonic wind tunnel with a chord length of approximately 1.5 feet (0.46 m) and a model span of approximately 2.8 feet (0.85 m). Results for the Reynolds number tested indicate that gap size should be no smaller than 2.5% system chord to avoid degradation in performance. A large overhang can adversely affect aerodynamic performance and lead to a loss of lift. Performance decreased if the strut was moved to any location other than the baseline condition. Results indicate that performance of high lift systems is more dependent upon the drag of the system than the high lift aerodynamics.**

## Nomenclature

| | | |
|---|---|---|
| $A$ | = | cross-sectional area |
| $C_l$ | = | 2D lift coefficient |
| $C_d$ | = | 2D drag coefficient |
| $C_m$ | = | 2D pitching moment coefficient |
| $c_n$ | = | individual chord of element $n$ |
| $c_{sys}$ | = | system chord length |
| $q$ | = | dynamic pressure |
| $P$ | = | pressure |
| $Re$ | = | Reynolds number |
| $S$ | = | total model wetted surface area |
| $T$ | = | temperature |
| $t/c$ | = | thickness-to-chord ratio |
| $V_\infty$ | = | freestream velocity |
| $x$ | = | Cartesian coordinate parallel to freestream flow |
| $y$ | = | Cartesian coordinate orthogonal to freestream flow |
| $\alpha$ | = | angle of attack |
| $\delta_n$ | = | absolute deflection angle of flap $n$ |
| $\delta_{rel,n}$ | = | relative deflection angle of flap $n$ |
| $\mu_{amb}$ | = | ambient dynamic viscosity |
| $\rho_{amb}$ | = | ambient density |

*Graduate Research Fellow, AIAA Student Member.
†Graduate Research Assistant
‡Associate Professor, AIAA Senior Member.

# I. Introduction

The goal of the research presented in this paper was to experimentally test the aerodynamic performance of various multielement airfoil configurations for use in the root section of large-scale (10-MW) wind turbines. Multielement airfoil design is complex, and aerodynamic performance is sensitive to geometric arrangement. Motivation for this project was driven by two primary factors, namely increased aerodynamic performance and improved structural integrity of the blade. Conflicts exist between structural requirements and aerodynamic performance.[1] A strong structure, contained in a thick airfoil, must exist at the root to support the aerodynamic loads as well as the weight of the blade. A thick airfoil can reduce aerodynamic performance compared with a thinner airfoil.

## A. Previous Work

Experimental studies of multielement airfoils were first performed in the 1940s, as discussed by the classic 2-D tests by Abbott and von Doenhoff[2] and supplemented by Jacobs, et al.[3] As discussed by Smith in 1975,[4] numerous effects govern the flow around high-lift multielement airfoil systems. Previous work studied aircraft multielement airfoil configurations which are only required during takeoff and landing. Multielement airfoils on aircraft are typically stored in the main element during cruise as shown below in Fig. 1. Wind turbine airfoils are mainly designed based on tip speed ratio at one angle of attack and can be point-designed for wind turbines as the flap does not need to retract into the main element as conventional aircraft do during cruise. Consequently, design and analysis efforts can be focused on the aerodynamics of the multielement airfoil configuration.

Aerodynamics of high lift systems are sensitive to the location and size of the gap between elements as well as the relative deflection angle. In general, a smaller gap accelerates the flow more rapidly while a larger gap does not accelerate the flow as much. However, confluent boundary layers and complex wake interactions can adversely affect the performance of the system if the gap is too small.[5] A smaller gap increases the magnitude of the suction peak of the flap and may reduce drag compared with a larger gap configuration.[6,7] Small gaps may reduce or eliminate separation over the flap but may also be more sensitive to stall than large gap configurations.[5,7] Previous research indicates that the best gap size is between 1.3% and 2.0% of system chord.[7–9]

Performance as a result of the overhang of the flaps has not been studied in as much detail as the effect of the gap. A positive overhang corresponds to an element that is tucked under the forward element while a negative overhang indicates the leading edge of an element is aft of the trailing edge of the forward element. The location of the flap was first discussed by Smith in 1975.[4] According to previous research, the best overhang value is approximately $-0.25\%$, which indicates the leading edge of the flap is behind the trailing edge of the forward element.[8] If the overhang is too far behind the trailing edge, the flow will not be accelerated around the leading edge of the flap, and the flap will not create as much lift as compared with a case having a smaller overhang.[8,9]

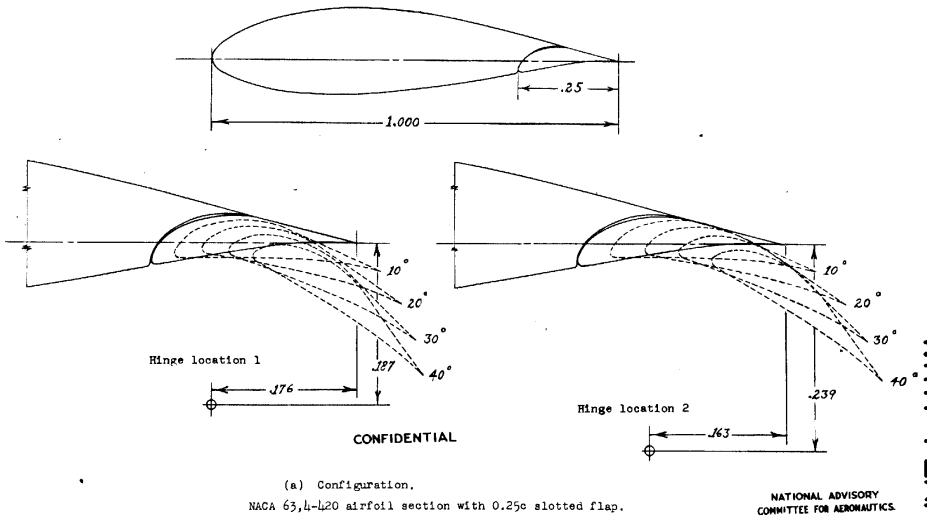


**Figure 1. Conventional multielement airfoils for use on aircraft.[2]**

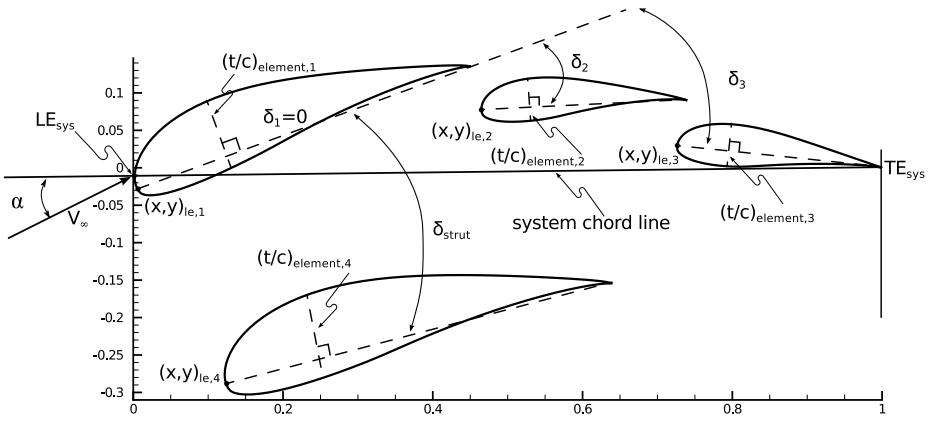


**Figure 2. Absolute coordinate system for multielement airfoil tests.**

The design of high-lift multielement airfoils has been performed with various different methods. Ragheb, et al.[10] used the inverse conformal mapping PROFOIL/MFOIL suite of programs to design the high lift airfoil system tested in this research project. Inverse viscous Navier-Stokes optimization codes have been employed to optimize the multi-element airfoil system for high lift.[11,12] The design of high-lift multielement airfoils must also consider the effect of the wakes. Wake interactions that are off the surface of multielement airfoils can be highly complex and difficult to predict and measure. Spreading and merging wakes shed from the different elements can have a strong effect on the pressure field, and large pressure gradients can cause wake bursting, or off-the-surface flow separation. These effects have been studied both experimentally and computationally.[4,5,12–24]

## B. Project Overview and Coordinate Systems

Numerous configurations of a multielement airfoil system were tested in this research. It is important to note that the multielement system was treated as a replacement for a thick single-element airfoil. An aggressive well-separated airfoil, the MFFS-026 designed by Ragheb, et al. [10] was chosen for this experiment. The main element of the system is coupled with two flaps and an additional element known as the "strut" was located below the upper three elements. Structural support for the system would be incorporated into a spar cap placed in the main element and a spar cap placed in the strut. No shear web would exist between the main element and the strut. The strut was primarily designed to act as a fairing around a spar cap and not a lifting element.

A coordinate system was developed to define the location of each element (see Fig. 2). A system chord length of unity was defined for the baseline case. Test cases that involved moving the flaps were analyzed as cases with chord lengths greater than or less than unity. The leading edge of the multielement system $(LE_{sys})$ did not correspond to the leading edge of the main element, but rather it was defined as the point furthest away from the trailing edge of the system and was set at the origin. The trailing edge of the final flap was set on the system chord line of $y = 0$ and defined as the trailing edge of the system $(TE_{sys})$. Each element was located based upon the leading edge coordinate $(x,y)_{le,n}$ for the element. All flap deflections $\delta$ were defined relative to the chord line of the main element, and the deflection angle of the main element $\delta_1$ was defined as 0 deg. The system angle of attack $\alpha$ was defined as the angle between the freestream velocity $U_\infty$ and the system chord line.

Aerodynamic performance of the system is highly dependent on gap size and minimum gap location as well as deflection angles between the elements. The relative coordinate system, shown in Fig. 3, was used to define the system by parameters that govern the flow. The relative deflection angle of the main element $(\delta_{rel,1)}$ was defined relative to the main system chord line, and the strut deflection angle $(\delta_{rel,strut})$ was defined relative to the main element chord line. The location of the flaps was constrained by gap size and overhang distance. The gap size between elements $(gap_n)$ was defined as the distance from the trailing edge of element $n$ to the closest point on element $n+1$. The overhang distance $(overhang_n)$ between element $n$ and $n+1$ was defined as the distance from the leading edge of element $n+1$ to the trailing edge of $n$ projected along the chord line of element $n$, as shown in the lower portion of Fig. 3. Relative deflection angles $(\delta_{rel,n})$ were defined as the angle between the chord line of element $n+1$ and the chord line of element $n$. A positive deflection angle corresponded to a downward flap deflection. The location of the strut was defined by the leading edge coordinates of the strut and the deflection angle relative to the main element.

 2012-2892

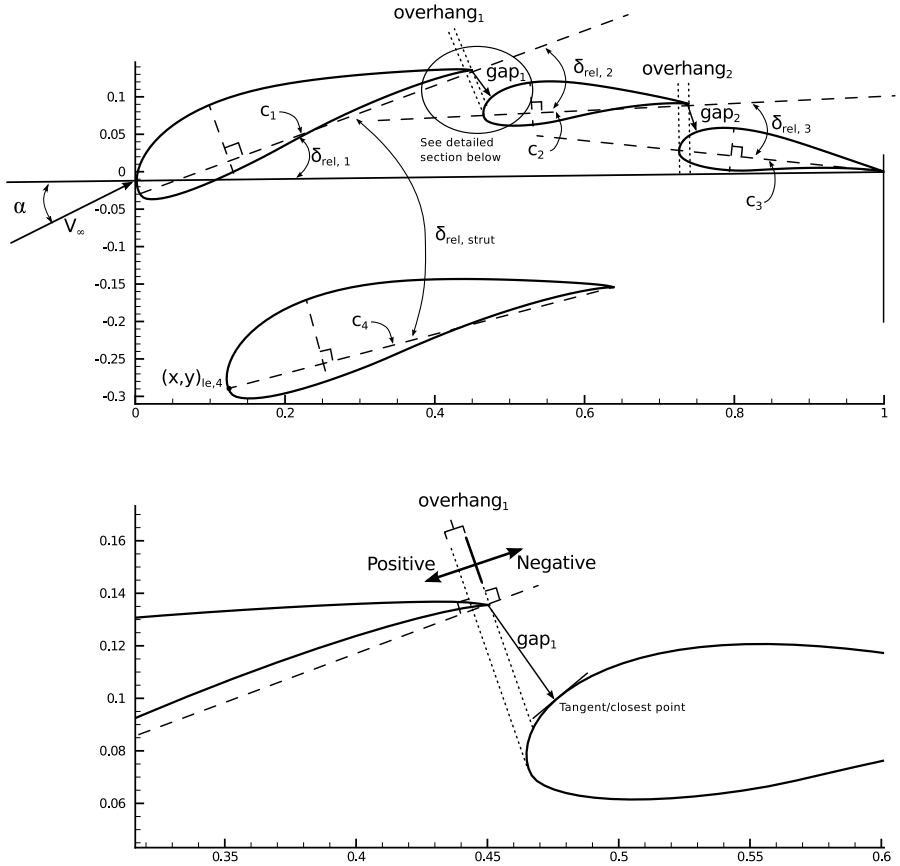


**Figure 3. Relative coordinate system for multielement airfoil tests.**

## II. Experimental Design

Aerodynamic tests were executed using the University of Illinois subsonic low-turbulence wind tunnel. The tunnel is a open-return-type wind tunnel with a rectangular test section measuring 2.8 ft (0.85 m) by 4.0 ft (1.22 m) along a downstream distance of 8.0 ft (2.44 m). The downstream location of the test section is 0.5 in (1.3 cm) wider than the upstream end to account for boundary layer growth along the walls. The contraction ratio of the tunnel is 7.5:1. A schematic of the wind tunnel is displayed below in Fig. 4. To ensure good flow quality, the air passes through a 4-in (10.2 cm) thick honeycomb mesh and also four stainless steel screens. The presence of these screens and flow conditioning reduces the empty test section turbulence intensity to less than 0.1% at all operating speeds.

The speed of the tunnel was set by a five-bladed metal fan driven by a 125-HP AC motor controlled by an ABB ACS 600 Low Voltage AC Drive. A maximum fan speed of 1,200 RPM creates an empty test section flow speed of approximately 165 mph (74 m/sec) or a maximum Reynolds number based on an 18-in (0.46 m) chord of approximately $2\times10^6$. The Reynolds number was computer controlled to within 0.5% during all tests.

The location of the flaps was controlled through the use of a custom-designed Flap Positioning System (FPS). The system was comprised of two sets of traverse systems. A traverse supported each flap on the top and on the bottom of the wind tunnel. Each flap was able to independently traverse in the $x_{tunnel}$ and $y_{tunnel}$ directions as well as rotate in $\delta$. A detailed photograph of one of the miniature traverses is shown below in Fig. 5. The *x*-*y* position of the traverse was controlled with a 1/4-20 ACME-threaded precision rod and was manually rotated by a hex key on the end of the rod. As shown below in Fig. 6, the location of the flaps was set on the top and bottom of the model, and the positions were monitored to ensure the model was not misaligned. A worm drive was used to rotate a 40-deg sector gear that set the flap deflection. The rotary position was set by the user rotating the sector gear or by using an Excitron SM20-30 micro stepper motor that was controlled by an Excitron 2A-TTL bipolar controller.

The position of the traverses in the linear and rotary directions was monitored through the use of ten MicroE Mercury 1500S-40 optical encoders. Eight encoders were used to monitor the *x* and *y* positions on the top and bottom of each of the two flaps, and two encoders were used to measure the angle of the two flaps. The linear position had a

resolution of 0.5 $\mu$m ($1.97 \times 10^{-5}$ in) and an accuracy of $\pm$ 3 $\mu$m (0.00012 in), and the rotary position was measured to a resolution of 39.6 arc-seconds (0.011 deg) and an accuracy of $\pm$ 3.9 arc-seconds (0.0011 deg).

# III. Results

Quantitative aerodynamic performance data were collected for the well-separated family of airfoils. Different configurations of the main-flap-flap-strut multielement airfoil system were named well-separated configurations. The well-separated configurations tested in the wind tunnel were all related to the baseline MFFS-026 airfoil system designed by Ragheb and is similar to the MFFS system discussed by Ragheb, et al.[10] Many well-separated configurations were generated by systematically varying gap size, overhang distance, strut deflection angle, and strut location. A four-element system consisting of a main element, two flaps, and a strut, was tested. The chord length of the main element was 11.50 in, the strut measured 7.84 in, and the flaps measured 3.50 in and 3.00 in for the first and second flap respectively. Model surface area, $S$, was defined as the total wetted area on the upper and lower surfaces of all four elements. System chord length of the baseline configuration was 17.53 in. Nondimensionalization and tunnel corrections used the baseline chord length of 17.53 in as the characteristic length. Data collected in the wind tunnel included $C_l$, $C_d$, and $C_m$. Methods presented by Barlow, et al.[25] were used to correct the wind tunnel measurements for wind tunnel wall effects. It is noted that all tests were performed at a Reynolds number of $0.975 \times 10^6$.

## A. Baseline Results

Tests were performed on the baseline WS-1 configuration, and the measured drag polar and lift curve are presented in Fig. 7. The value of $C_{l,max}$ is 1.72 for $\alpha = 13$ deg. Wake profiles show that the flow over the entire system was separated at $\alpha = 0$ deg. The main three-element system attached at an angle of $\alpha = 1$ deg while the strut flow did not attach until $\alpha = 6$ deg. A large drop in $C_d$ is noted where the flow over the strut attached at $\alpha = 6$ deg. Stall characteristics were gradual and gentle, which suggest a thin airfoil stall or a trailing edge stall. The linear region of the $C_l$-$\alpha$ curve extends from an angle of attack of 1 deg through 11 deg. Relative coordinates for the baseline configuration are presented in Table 1.

## B. Cross-Case Analysis

Data from a carefully constructed test matrix were analyzed to understand the relationship between each independent parameter and the aerodynamic performance. Tests were performed in an effort to understand the effect of gap size, overhang distance, and strut location on the aerodynamic performance of the airfoil system. The gap and overhang distances were changed using the previously discussed flap positioning system. Numerous different "cases" were generated by systematically varying one or at most two independent parameters. The parameters included gap size, overhang distance, strut leading edge location, and strut deflection angle. Flaps were set at a constant flap deflection for all tests. Data are presented for multiple different airfoil systems at a fixed angle of attack.

The cases studied captured independent multielement effects with emphasis on gap size and overhang distance. A summary of the cases of configurations tested is presented in Table 2. Some cases included parameter sweeps while

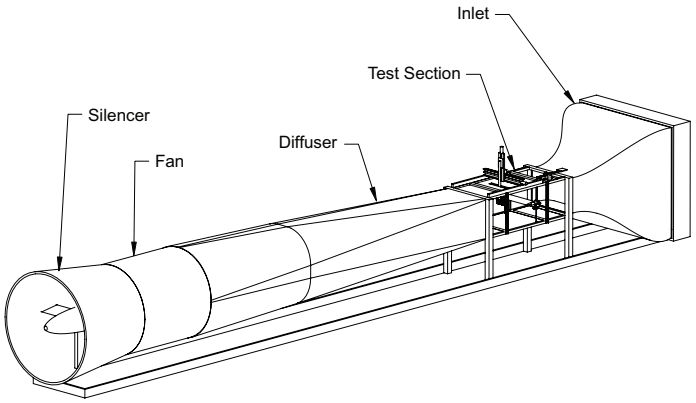


**Figure 4. University of Illinois low-speed low-turbulence subsonic wind tunnel.**

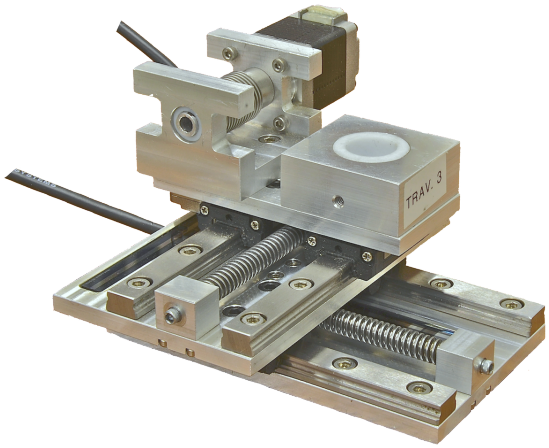


**Figure 5. Custom-designed flap positioning traverse to set $x$-$y$ position and $\delta$ (flap angle drive omitted).**


**Figure 6. Location of four traverses relative to wind tunnel model.**

other cases did not. As previously mentioned, each case consisted of a single parameter which was altered. Tests performed in Cases 1 and 2 measured the effect of overhang distance at two different gap sizes. Case 3 captured the effect of strut deflection angle on the aerodynamic performance of the system. Performance of the system as a function of gap size was captured in Cases 7 and 8 while the location of the strut was tested in Cases 8 through 13. The focus of Case 8 was to study the effect of the gap size if the strut was not in its home position. Data collected in Cases 9 through 13 (supplemented by data in Cases 2, 4, and 8) studied the effect of the strut location on the aerodynamic performance.

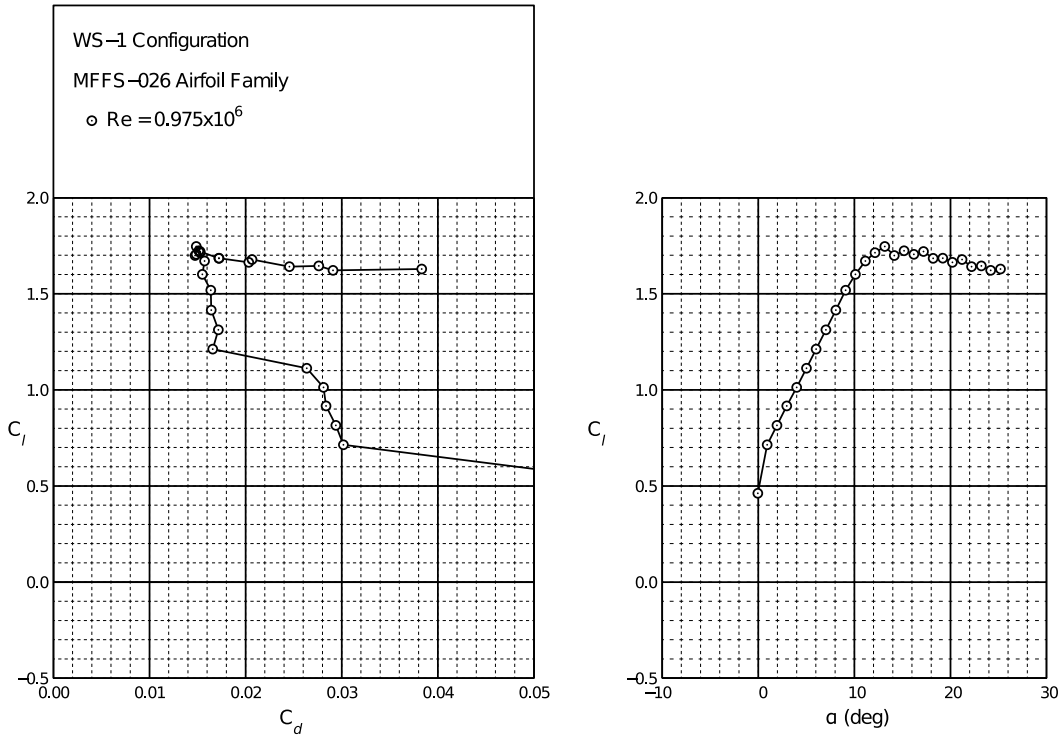


**Figure 7. Results of baseline configuration at $Re = 0.975 \times 10^6$.**

### *1. Effect of Gap Size*

As shown in Fig. 8(a), the gap size of the two flaps affects the lift of the entire multielement system. The two gap sizes were the same value such that $gap_1 = gap_2$ while the overhang for each element was defined as $overhang_1 = overhang_2 = 0.015$ (Table 2, Case 7). A peak in the $C_l$ vs $gap$ curve is observed at a gap size of 0.020. The rate of decrease of $C_l$ is greater at small gaps than at larger gaps. The drag is also affected by the size of the gap between the

**Table 1. Baseline Parameters Defining the WS-1 Four-Element Configuration**

| | |
|---|---|
| $\delta_{rel,1}$ | 13.24 deg |
| $c_1$ | 11.50 in |
| $overhang_1$ | 0.0217 |
| $gap_1$ | 0.0303 |
| $\delta_{rel,2}$ | 17.14 deg |
| $c_2$ | 3.50 in |
| $overhang_2$ | −0.0082 |
| $gap_2$ | 0.0303 |
| $\delta_{rel,3}$ | 8.74 deg |
| $c_3$ | 3.00 in |
| $x_{le,strut}$ | 0.1716 |
| $y_{le,strut}$ | −0.2682 |
| $\delta_{rel,strut}$ | −6.50 deg |
| $c_4$ | 7.84 in |

**Table 2. Well-Separated Airfoil Test Matrix**

| Cases | $overhang_n$ [$\%c_{sys}$] | $gap_n$ [$\%c_{sys}$] | $\delta_2$ [deg] | $\delta_3$ [deg] | $x_{strut}$ [$\%c_{sys}$] | $y_{strut}$ [$\%c_{sys}$] | $\delta_{strut}$ [deg] |
|---|---|---|---|---|---|---|---|
| 1 | −0.010 to 0.020 | 0.030 | 17.1 | 13.0 | 0.172 | −0.268 | −6.5 |
| 2 | −0.005 to 0.020 | 0.025 | 17.1 | 13.0 | 0.172 | −0.268 | −6.5 |
| 3 | −0.005 to 0.020 | 0.025 | 17.1 | 13.0 | 0.182 | −0.286 | −16.5 |
| 4 | 0 to 0.010 | 0.025 | 17.1 | 13.0 | 0.158 | −0.212 | −6.5 |
| 5 | −0.005 to 0.010 | 0.025 | 17.1 | 13.0 | 0.185 | −0.323 | −6.5 |
| 6 | −0.005 to 0.010 | 0.025 | 17.1 | 13.0 | 0.240 | −0.310 | −6.5 |
| 7 | 0.015 | 0.01 to 0.035 | 17.1 | 13.0 | 0.172 | −0.268 | −6.5 |
| 8 | 0.015 | 0.01 to 0.035 | 17.1 | 13.0 | 0.185 | −0.323 | −6.5 |
| 9 | 0.010 | 0.025 | 17.1 | 13.0 | 0.214 | −0.199 | −6.5 |
| 10 | 0.010 | 0.025 | 17.1 | 13.0 | 0.103 | −0.225 | −6.5 |
| 11 | 0.010 | 0.025 | 17.1 | 13.0 | 0.116 | −0.281 | −6.5 |
| 12 | 0.010 | 0.025 | 17.1 | 13.0 | 0.227 | −0.254 | −6.5 |
| 13 | 0.010 | 0.025 | 17.1 | 13.0 | 0.164 | −0.247 | −6.5 |

different elements and results are plotted in Fig. 8(b). A local minimum in drag is observed at $gap_{1,2} = 0.015$ which is a slightly smaller gap size than the gap size with maximum lift. The drag is reduced by approximately 5% relative to the drag at $gap_{1,2} = 0.020$. Data at a gap size of 0.010 suggest a drag rise at small gap sizes; this effect may be driven by interacting boundary layers and wakes. In addition, the aerodynamic efficiency, $C_l/C_d|_\alpha$, as a function of gap size is plotted in Fig. 8(c). A maximum in the lift-to-drag-ratio is observed at a gap size of 0.015, which is the gap size with minimum drag. The lift-to-drag ratio at the gap size with maximum lift ($gap_{1,2} = 0.020$) is 78.2, a 4.6% reduction relative to the point with maximum $C_l/C_d|_\alpha$. A reduction in $C_l/C_d|_\alpha$, driven primarily by a reduction in lift, is observed at small gap sizes. Similar trends were observed for other angles of attack.

### 2. *Effect of Overhang Distance*

Tests were performed to isolate the effect of the overhang distance on the aerodynamic performance, and results are presented in Fig. 9. The overhang distance was the same for both flaps (Table 2, Case 2). Lift as a function of overhang is presented in Fig. 9(a). The relationship is more complex than that of the gap effect on the lift. A maximum value of $C_l$ is observed at $overhang_{1,2} = -0.005$. As noted in Fig. 3, a negative overhang is a distance in which the leading edge of element $n$ is aft of the trailing edge of element $n-1$. Positive overhang distances adversely affect the lift produced by the system. The drag of the multielement airfoil system is also a function of the overhang distance and results are shown in Fig. 9(b). The results show that larger positive overhangs have the lowest drag. A drag reduction of 5.6% exists at an overhang distance of 0.015 compared with no overhang. A sharp drag reduction is observed between 0.005 and 0.010. Lift-to-drag ratio as a function of overhang distance is plotted in Fig. 9(c). The $C_l/C_d|_\alpha$ at the overhang with maximum lift is 75.0 while $C_l/C_d|_\alpha$ in the low drag region is as high as 77.7. Additionally, the lift-to-drag ratio is locally minimized at an overhang of 0.005 which is the value with the highest drag. The observed trends show the effect of the low drag values has a greater effect on the aerodynamic efficiency than the benefit of increased lift.

### 3. *Effect of Strut Deflection Angle*

Data were collected with the gap and overhang at a constant value while the strut deflection angle was independently varied. The baseline deflection of the strut was −6.5 deg, and the strut could be deflected ±10 deg in the baseline *x-y* position. The strut was designed to act as a fairing and not as a lifting element. Lift as a function of strut deflection angle is presented in Fig. 10(a) (Table 2 Case 2 and 3). Total lift is increased for positive strut deflections as the strut transitions from a curved non-lifting fairing to a lifting element. In addition, the lift decreases as the strut deflection decreases because the strut produces negative lift. Deflection of the strut also affects the drag of the multielement airfoil

system, as noted in Fig. 10(b). A negative strut deflection angle causes the drag to increase dramatically relative to the baseline case, as noted for the cases with $\delta_{strut} = -16.5$ deg. This drag increase could be a result of flow separation on the strut or other multielement aerodynamic effects caused by the strut. The drag remains nearly constant for positive strut deflection angles. The combined effect of the strut deflection angle on the aerodynamic efficiency of the system is presented in Fig. 10(c). Negative deflection angles, due to the large drag rise and negatively lifting strut, decrease the value of $C_l/C_d|_\alpha$ relative to the baseline case. A positively deflected strut generates slightly more lift than the baseline case for approximately the same drag value which translates into a small $C_l/C_d|_\alpha$ increase at a positive strut deflection relative to the baseline case.

### *4. Effect of Strut Location*

The experimental setup allowed for the strut to be moved to eight separate locations (Table 2, Cases 2, 4-6 9-13). Movement was permitted in a direction normal and/or tangential to the main element chord at a distance of 5.7% system chord. Movement was possible in any combination of up/down and fore/aft except forward and down as the wind tunnel balance support leg would have interfered with the strut spar. The label of $Strut_{u/d}$ corresponds to the location of the strut in the direction normal to the chord of the main element (up/down) while $Strut_{f/a}$ is the distance the strut was moved tangential to the main element chord line. A positive value of $Strut_{u/d}$ indicates the strut was moved toward the main element, and a positive value of $Strut_{f/a}$ indicates the strut was moved aft of the original location. As shown in Fig. 11(a), the location of the strut has an effect on the $C_l$ of the system. Lift is the highest when the strut is in the baseline position and is reduced in all other seven locations. No clear trend exists between cases at a constant up/down location. Drag values of the eight different strut location cases are presented in Fig. 11(b). Drag is reduced for cases in which the strut is moved away from the main element (moved down). In general, drag is lowest for a given main element chord normal location when the fore/aft location is 0. Finally, the $C_l/C_d|_\alpha$ of the airfoil system as a function of strut location is presented in Fig. 11(c). The $C_l/C_d|_\alpha$ is maximized when the strut is in the baseline fore/aft location and moved away from the main element of the system. The lift to-drag-ratio in the baseline case is 2.9% less than the best observed case.

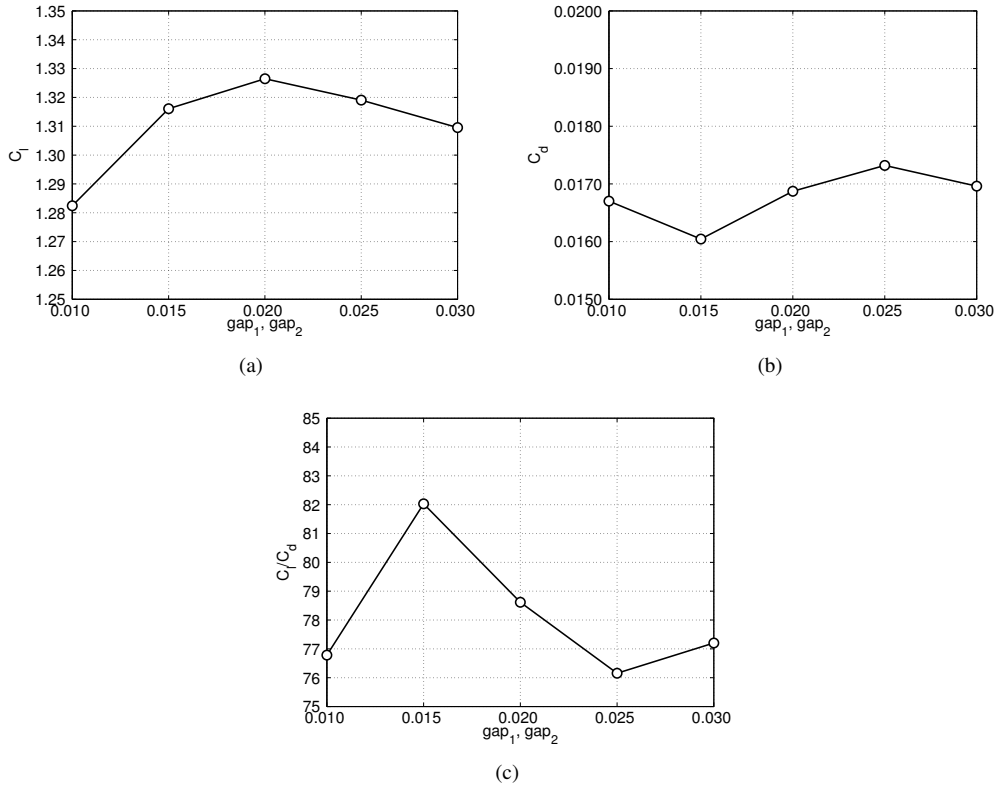


**Figure 8. Effect of gap size for MFFS-026 airfoil at $\alpha = 6$ deg at constant overhang: (a) lift, (b), drag, and (c) lift-to-drag ratio.**

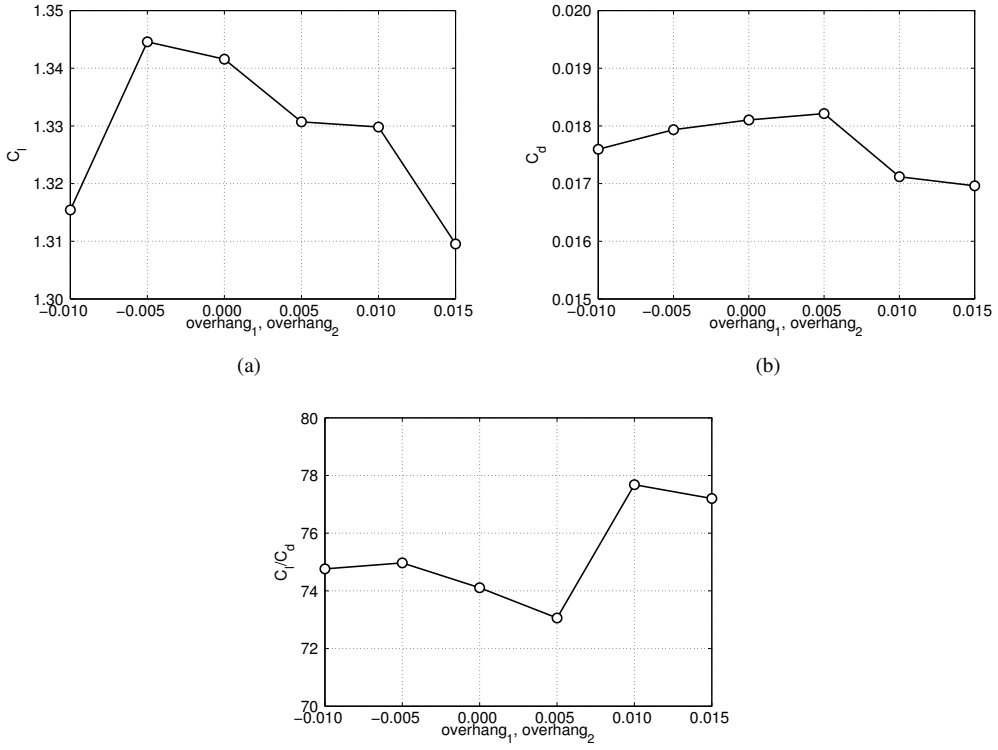


**Figure 9. Effect of overhang distance for MFFS-026 airfoil at $\alpha = 6$ deg and constant gap: (a) lift, (b), drag, and (c) lift-to-drag ratio.**

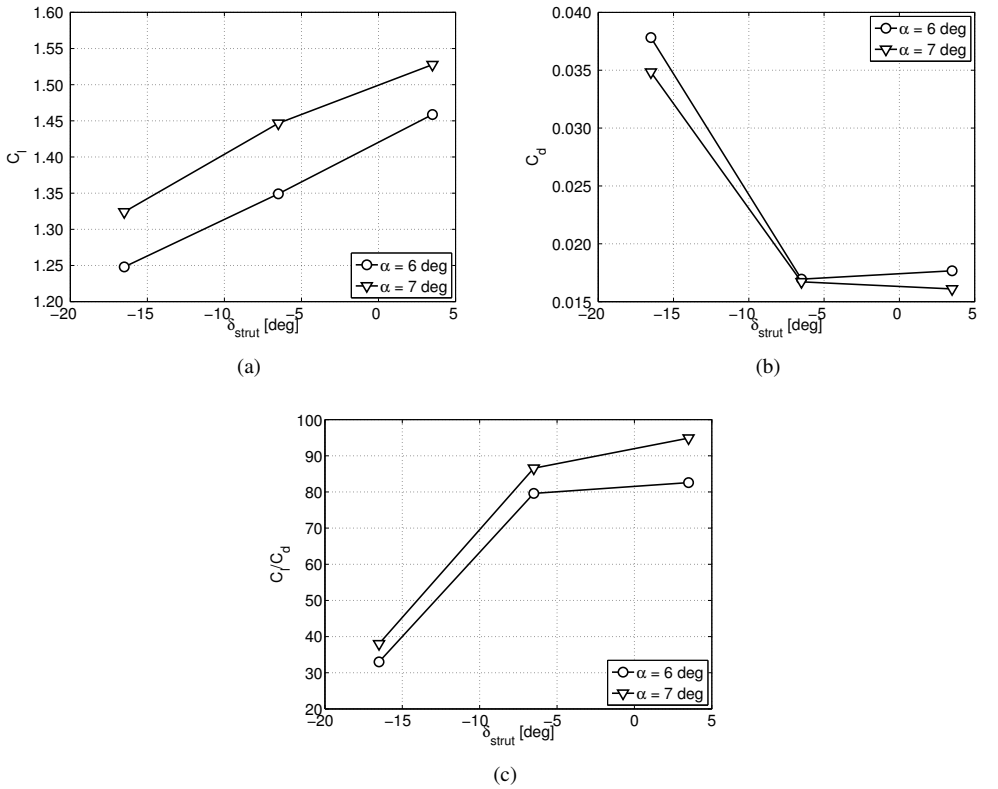


**Figure 10. Effect of strut deflection angle for MFFS-026 airfoil at constant gap and constant overhang: (a) lift, (b), drag, and (c) lift-to-drag ratio.**

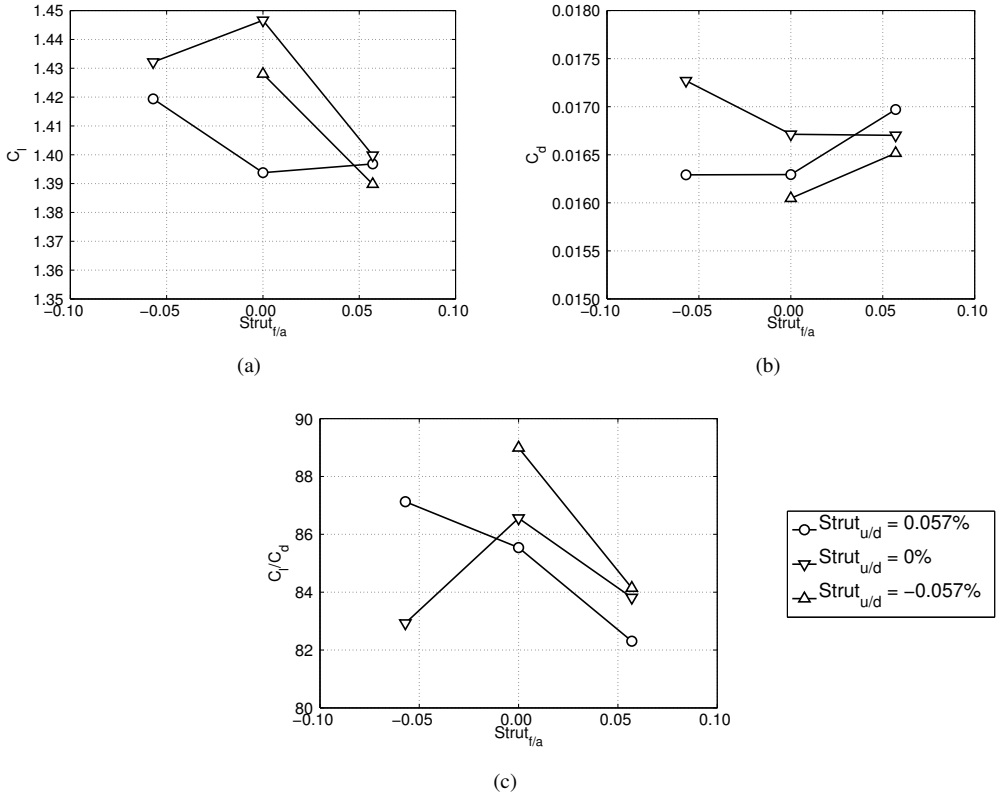


**Figure 11. Effect of strut location for MFFS-026 airfoil at constant gap and constant overhang: (a) lift, (b), drag, and (c) lift-to-drag ratio.**

### *5. Coupled Effect of Strut Deflection Angle and Overhang Distance*

The combined effect of $\delta_{strut}$ and overhang distance was captured and analyzed (Table 2, Cases 2-3). Airfoil configurations were tested at a strut deflection of $-6.5$ deg (the baseline deflection angle) and $-16.5$ deg. A range of overhang distances varied from $-0.005$ to 0.02. All tests were performed at a constant gap size of 0.025. The combined effect on lift is plotted in Fig. 12(a). The effect of the strut deflection angle on $C_l$ is larger than the effect of the overhang distance. As previously observed in Fig. 9(a), overhang distance has a minimal effect on the lift of the multielement airfoil system. Drag as a function of strut deflection angle and overhang distance is shown in Fig. 12(b). The deflection angle of the strut affects the drag of the multielement system more than the overhang distance, and drag values at a negative deflection angle are more than twice as high as the baseline deflection case. A positive overhang may reduce the drag of the system compared with a negative overhang distance. Aerodynamic efficiency at various strut deflection angles and overhang distances is plotted in Fig. 12(c). It is noted that the overhang distance has a minimal effect on $C_l/C_d|_\alpha$. The strut deflection angle greatly affects the value of $C_l/C_d|_\alpha$. This reduction in aerodynamic efficiency is primarily driven by the increase in drag for the reduced deflection angle.

### *6. Coupled Effect of Strut Location and Gap Size*

The combined effect of gap size and strut position was also measured. Cases were generated at a constant overhang distance of 0.015 and a gap size from 0.01 to 0.035. The strut was place in the baseline position and also moved away from the main element chord line. The coupled effect of lift is presented in Fig. 13(a). In general, lift decreases for gap sizes less than 0.02, and a local maximum is observed at 0.02. The lift of the system decreases for gap sizes between 0.02 and 0.03 but increases at gap size of 0.035 relative to the lift at a gap size of 0.03. Data were not collected at gap sizes greater than 0.035. Figure 13(b) shows the effect of strut location and gap size on the drag of the system. Both parameters affect the drag, and the relationship between the two parameters is not clear. The drag for the baseline configuration is minimized at a gap size of 0.015 and maximized at a gap size of 0.025, as presented in Fig. 8(b). However, drag for the case in which the strut was moved down is minimized at a gap size of 0.02 and maximized at a gap size of 0.015. The combined aerodynamic efficiency as a function of strut location and gap size is presented in Fig. 13(c). No clear trend was observed between the strut deflection angle and overhang distances. A maximum in

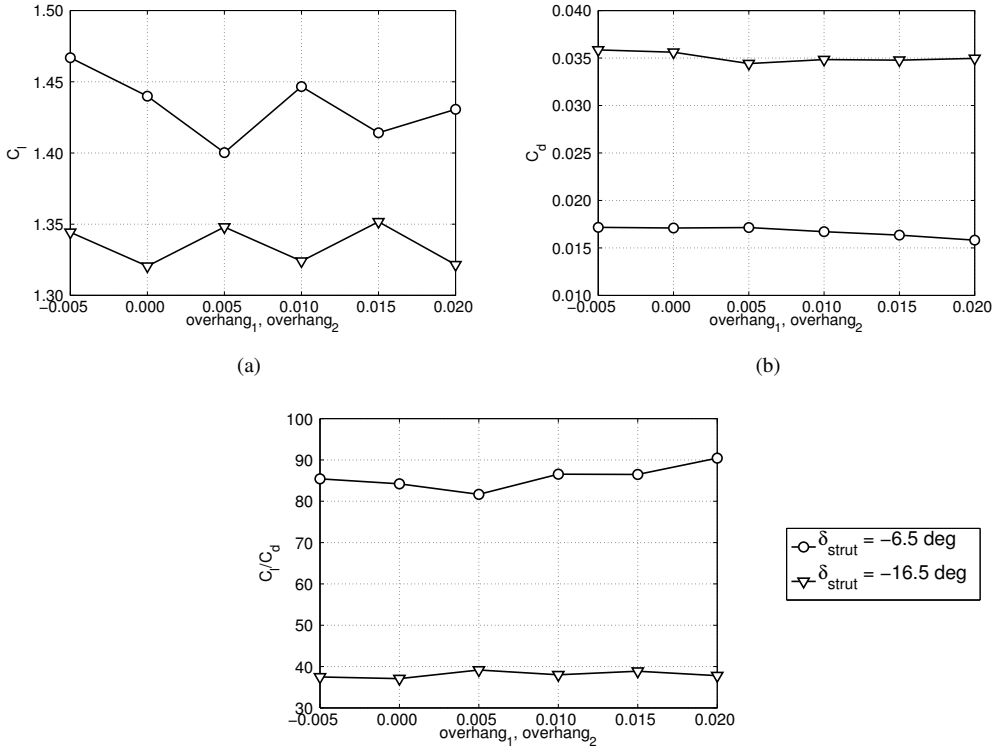


**Figure 12. Effect of strut deflection angle and overhang distance for MFFS-026 airfoil at $\alpha = 6$ and 7 deg: (a) lift, (b), drag, and (c) lift-to-drag ratio.**

$C_l/C_d|_\alpha$ is observed between 0.015 and 0.02 for both locations of the strut. A sharp reduction in lift-to-drag ratio is observed for gap sizes slightly smaller than that for which the maximum occurred.

## IV. Concluding Remarks

Wind tunnel tests were carried out on a multielement airfoil configuration for application to the root section of a 10-MW scale wind turbine blade. Tests were performed on the four-element MFFS-026 multielement airfoil system that was designed to replace a thick, aerodynamically inefficient, single-element airfoil near the root section of large scale wind turbines. The multielement airfoil system consisted of a main element, two flaps, and a lower strut airfoil element. A strut was added for additional structural rigidity. Wind tunnel tests were performed in the University of Illinois $3 \times 4$ low-speed low-turbulence wind tunnel. A flap positioning system was designed and fabricated to move the flaps over a range of positions. Tests were performed to capture the dependency of specific parameters on the performance of the system. Parameters of interest included gap size, overhang distance, strut location, and strut deflection angle.

Numerous trends were observed in the results. The drag of the system affected the $C_l/C_d$ of the system more than the total lift. The results show that the best gap size is approximately 2.5% system chord while the overhang with the highest $C_l/C_d$ was approximately $-0.25\%$ system chord. Trends show that the best gap size is not constant with different overhang distances. Similarly, the best overhang distance varies with gap size. The best gap size at one strut location is different than the best gap size at a different strut location. All relative coordinates are coupled and all must be considered in the design process.

Conclusions indicate that a multielement airfoil system must be designed as one system. Different elements cannot be designed independently and then simply placed at a certain gap size or overhang distance. A further study could be done by incorporating an inverse viscous design routine to design the multielement system while avoiding viscous phenomena such as merging and interacting wakes. This method would also find the best gap size and overhang distance for each multielement airfoil system.

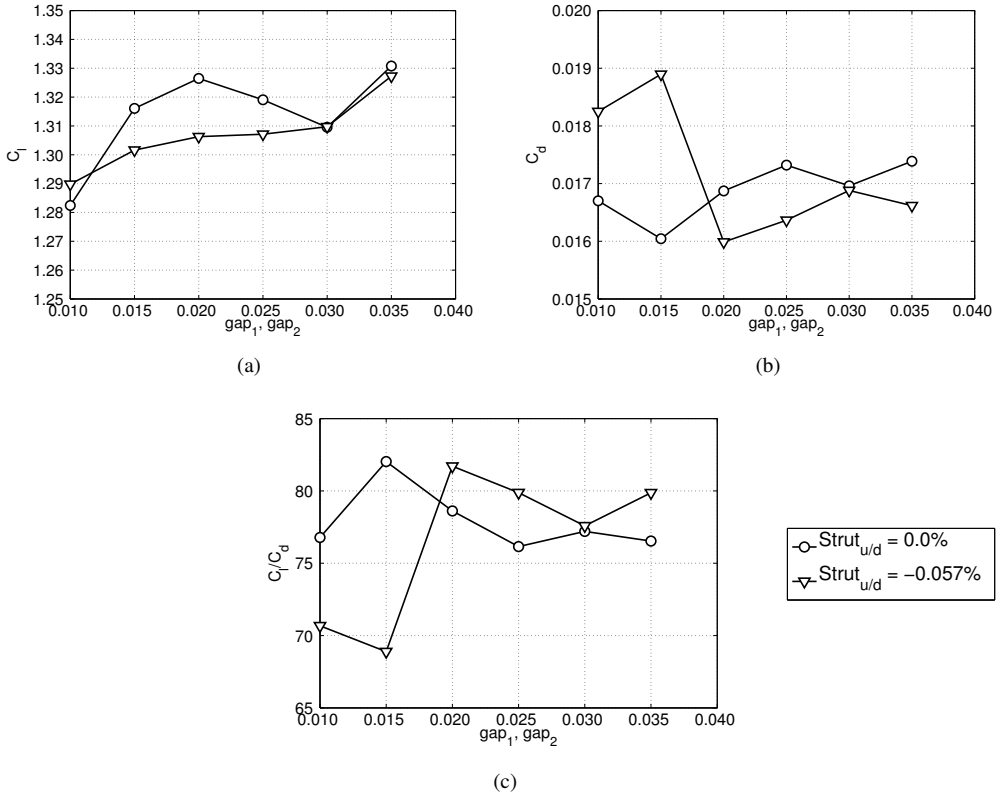


**Figure 13. Effect of strut location and gap size for MFFS-026 airfoil at $\alpha = 6$ at constant overhang: (a) lift, (b), drag, and (c) lift-to-drag ratio.**

## Acknowledgments

Support for this research project was provided by National Science Foundation graduate research fellowship grant number 07-15088, GE Energy, and the UIUC Department of Aerospace Engineering.

## References

[1]Wirz, R. E. and Johnson, P. M., "Aero-Structural Performance of Multiplane Wind Turbine Blades," AIAA 2011-3025, Applied Aerodynamics Conference, Honolulu, HI, 2011.

[2]Abbott, I. and Miller, R. B., "Tests of a Highly Cambered Low-Drag Airfoil Section with a Lift-Control Flap," NASA TR 74843, 1943.

[3]Jacobs, E. N., Abbott, I., and Davidson, M., "Preliminary Low-Drag-Airfoil and Flap Data from Tests at Large Reynolds Numbers and Low Turbulence," NACA TM 74843, 1943.

[4]Smith, A. M. O., "High-Lift Aerodynamics," *Journal of Aircraft*, Vol. 12, No. 6, 1975, pp. 501–530.

[5]Spaid, F. W., "High Reynolds Number, Multielement Airfoil Flowfield Measurements," *Journal of Aircraft*, Vol. 37, No. 3, 2000, pp. 499–507.

[6]Cerra, D. F. and Katz, J., "Design of a High-Lift, Thick Airfoil for Unmanned Aerial Vehicle Applications," *Journal of Aircraft*, Vol. 45, No. 5, 2008, pp. 1789–1793.

[7]Ashby, D. L., "Experimental and Computational Investigation of Lift-Enhancing Tabs on a Multi-Element Airfoil," NASA TR 110432, 1996.

[8]Lin, J. C. and Doninik, C. J., "Parametric Investigation of a High-Lift Airfoil at High Reynolds Numbers," *Journal of Aircraft*, Vol. 34, No. 4, 1997, pp. 485–491.

[9]Coiro, D. P., Nicolosi, F., and Grasso, F., "Design and Testing of Multi-Element Airfoil for Short-Takeoff-and-Landing Ultralight Aircraft," *Journal of Aircraft*, Vol. 46, No. 5, 2009, pp. 1795–1807.

[10]Ragheb, A. M. and Selig, M. S., "Multi-Element Airfoil Configurations for Wind Turbines," AIAA 2011-3971, AIAA Applied Aerodynamics Conference, Honolulu, HI, 2011.

[11]Howe, G. D., "Optimization of 2-D Flap Geometry Using Matlab and Fun3D," AIAA 2011-823, AIAA Aerospace Sciences Meeting, Orlando, FL, 2011.

[12]Rogers, S. E., "Progress in High-Lift Aerodynamic Calculations," *Journal of Aircraft*, Vol. 31, No. 6, 1994, pp. 1244–1251.

[13]Nakayama, A., Kreplin, H., and Morgan, H., "Experimental Investigation of Flowfield About a Multielement Airfoil," *AIAA Journal*, Vol. 28, No. 1, 1988, pp. 14–21.

[14]Chin, V. D., "Flowfield Measurements about a Multi-Element Airfoil at High Reynolds Numbers," AIAA 93-3137, AIAA Fluid Dynamics Conference, Orlando, FL, 1993.

[15]Drela, M. and Giles, M. B., "Viscous-Inviscid Analysis of Transonic and Low Reynolds Number Airfoils," AIAA 86-1786, AIAA Applied Aerodynamics Conference, San Diego, CA, 1986.

[16]Drela, M., "Design and Optimization Method for Multi-Element Airfoils," AIAA 93-0969, AIAA Aerospace Design Conference, Irvine, CA, 1993.

[17]Bucci, G. S. and Sullivan, J. P., "An Experimental Simulation of High Lift Wake Flows at High Reynolds Number," AIAA 97-31787, AIAA Applied Aerodynamics Conference, Atlanta, GA, 1997.

[18]Cebeci, T., Besnard, E., and Chen, H. H., "Calculation of Multielement Airfoil Flows, Including Flap Wells," AIAA 96-0056, AIAA Aerospace Sciences Meeting, Reno, NV, 1996.

[19]Czerwiec, R. and Edwards, J. R., "Theory and Experiment of Multielement Airfoils - A Comparison," AIAA 2000-0985, AIAA Aerospace Sciences Meeting, Reno, NV, 2000.

[20]Hoffenberg, R. and Sullivan, J. P., "Simulation of High-Lift Wake Behavior," AIAA 97-0718, AIAA Aerospace Sciences Meeting, Reno, NV, 1997.

[21]Driver, D. M. and Mateer, G. G., "Wake Flow in Adverse Pressure Gradient," *International Journal of Heat and Fluid Flow*, Vol. 223, 2002, pp. 564–571.

[22]Hoffenberg, R. and Sullivan, J. P., "Measurement and Simulation of Wake Deceleration," AIAA 98-0522, AIAA Aerosciences Meeting, Reno, NV, 1998.

[23]Schneider, S., Campbell, B., Bucci, G., and Sullivan, J. P., "An Experimental Simulation of Flap Flow on Multielement Airfoils at High Reynolds Number," AIAA 94-2613, AIAA Aerospace Ground Testing Conference, Colorado Springs, CO, 1994.

[24]Hoffenberg, R., Sullivan, J. P., and Schneider, S., "Wake Measurements in a Strong Adverse Pressure Gradient," NASA TR 197272, 1995.

[25]Barlow, J. B., Rae, Jr., W. H., and Pope, A., *Low-Speed Wind Tunnel Testing*, Wiley-Interscience, 3rd ed., 1999.